THE JOURNAL OF PHYSICAL CHEMISTRY B

Article

pubs.acs.org/JPCB

Dynamic Responses and Initial Decomposition under Shock Loading: A DFTB Calculation Combined with MSST Method for β-HMX with Molecular Vacancy

Zheng-Hua He,[†,‡,§] Jun Chen,[§] Guang-Fu Ji,[†] Li-Min Liu,[*,‡] Wen-Jun Zhu,[*,†] and Qiang Wu[†]

[†]National Key Laboratory of Shock Wave and Detonation Physics, Institute of Fluid Physics, Mianyang 621900, Sichuan, China

[‡]Beijing Computational Science Research Center, Beijing 100084, China

[§]National Key Laboratory of Computational Physics, Institute of Applied Physics and Computational Mathematics, Beijing 100088, China

Supporting Information

ABSTRACT: Despite extensive efforts on studying the decomposition mechanism of HMX under extreme condition, an intrinsic understanding of mechanical and chemical response processes, inducing the initial chemical reaction, is not yet achieved. In this work, the microscopic dynamic response and initial decomposition of β-HMX with (1 0 0) surface and molecular vacancy under shock condition, were explored by means of the self-consistent-charge density-functional tight-binding method (SCC-DFTB) in conjunction with multiscale shock technique (MSST). The evolutions of various bond lengths and charge transfers were analyzed to explore and understand the initial reaction mechanism of HMX. Our results discovered that the C−N bond close to major axes had less compression sensitivity and higher stretch activity. The charge was transferred mainly from the N−NO_2 group along the minor axes and H atom to C atom during the early compression process. The first reaction of HMX primarily initiated with the fission of the molecular ring at the site of the C−N bond close to major axes. Further breaking of the molecular ring enhanced intermolecular interactions and promoted the cleavage of C−H and N−NO_2 bonds. More significantly, the dynamic response behavior clearly depended on the angle between chemical bond and shock direction.

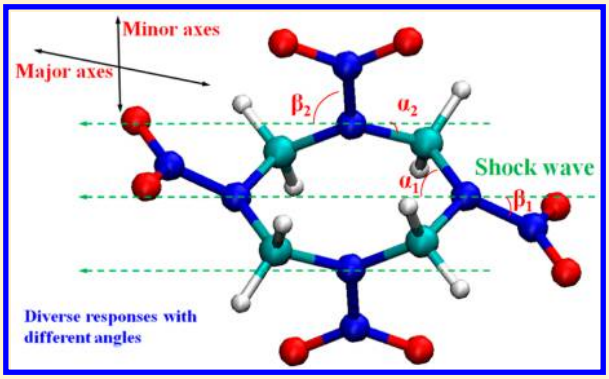

1. INTRODUCTION

Octahydro-1,3,5,7-tetranitro-1,3,5,7-tetrazocine (HMX), a typical nitramine explosive, has been widely used as an important component of various high performance compound explosives and rocket propellants, because of its thermal stability and high detonation velocity.[1−3] However, the intrinsic decomposition mechanism of HMX under shock loading is unclear yet after several decades of application. In fact, the shock compression process is not only a simple dynamic stress on energetic materials but also a simultaneous heating process. This complicated coupling interaction of mechanical and thermodynamic initiates the early chemical reaction, making the study of these energetic materials really difficult using experimental method. It is of great significance to develop a comprehensive understanding and description of the intrinsic chemical reaction mechanism at the atomic level to promote its further application.

In recent years, the fundamental properties, mechanical response, and thermodynamic behavior of HMX were reported based on a large number of experimental data and theoretical calculations.[4−18] HMX was known to exist into four crystalline phases: α, β, γ, and δ. The β polymorph was the most dense (∼1.96 g·cm^{-3}) and thermodynamically stable under ambient condition.[5−8] β-HMX had the least impact sensitivity among these four configurations and would convert into δ phase at higher temperature (∼413 K) or pressure (∼4 GPa).[8−10] The condensed phase detonation velocity and pressure of HMX under steady detonation were reported, being 9.1 km·s^{-1} and 39 GPa,[12] respectively. The initial reaction sites of HMX and the main decomposition products had been investigated both for gaseous and crystalline HMX.[10,19−27] Three different primary initial reaction models had been proposed for thermal decomposition of HMX: (I) the homolytic cleavage of N−NO_2 to form NO_2, (II) HONO elimination by interaction between H and NO_2, and (III) the nitro−nitrite isomerization to form NO. However, the initial reaction mechanism was obviously different between the thermal and shock conditions. Ge et al.[20,26] discovered that the homolytic cleavage of N−NO_2 bond was obviously suppressed when the shock velocity was above 10 km·s^{-1} and the fission of the C−H bond was the primary

Received: May 28, 2015
Revised: July 6, 2015
Published: July 28, 2015

DOI: 10.1021/acs.jpcb.5b05081
J. Phys. Chem. B 2015, 119, 10673−10681

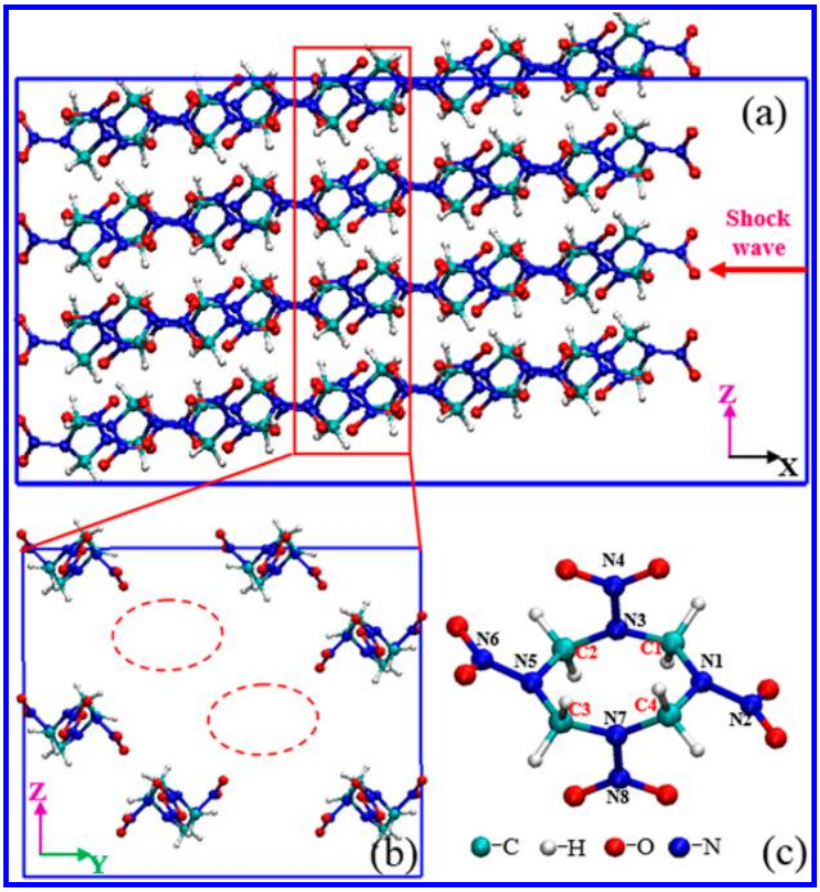

Figure 1. Slab model of 5 × 2 × 2 supercell structure of β-HMX: (a) (1 0 0) surface with 5 Å vacuum, (b) two-molecule vacancy, and (c) β-HMX molecular structure.

pathway for HMX decomposition at the initial stage. Zhu et al.[23] reported that the decomposition of HMX triggered by the breaking of the N−O bond and the opening of the molecular ring under shock velocity of 6.5 km·s^{-1}. Many experimental and theoretical studies suggested that the N−NO_2 bond fission had the lowest energy barriers.[10,22] However, the N−N bond was significantly compressed at high pressure.[13,16] It was still contradicted which one was the dominant pathway among these reaction models.

Recently, the effect of defects and surface to initial reaction process of condensed phase HMX decomposition attracted more attention.[22,25,28−33] Sharia and Kuklja[22,30] found the surface and vacancy caused a nonequilibrium vibration of N−NO_2 bond, which would decrease the potential barrier of homolytic cleavage of the N−NO_2 bond. Zhou and Huang[25] suggested that molecular vacancies could help to decrease the activation energy barrier and increase the reaction rate. Wen et al.[29] reported that the twined crystal HMX was remarkably more sensitive to shock. All of the results indicated that the initial reaction behavior of HMX strongly depended on the local crystal structure. It was necessary to further study the shock response of HMX with surface and defects.

The early dynamic response behavior of HMX under shock loading was very important for understanding the initial decomposition mechanism, which just directly affected the ignition process, reaction pathways, and thermal energy release of the explosive. However, this process was seldom reported at the previous works. In this work, we have performed quantum-based molecular dynamics (MD) calculations for β-HMX with (1 0 0) surface and molecular vacancy under shock loading, combined with the multiscale shock technique (MSST), to reveal the dynamic response properties and initial reaction mechanism of β-HMX during the early compression process. In our studies, the diverse compression and stretch behaviors of the same kind of bonds were compared and the intrinsic reason for the different responses was analyzed, which had never been reported at previous works. The initial decomposition mechanism was proposed and further understood by analyzing dynamic charge transfer at the electronic level. Our studies not only uncovered a novel and general reaction mechanism for β-HMX under shock loading but also served as a new angle to explore and understand the dynamic response and initial decomposition of energetic materials.

2. COMPUTATIONAL DETAILS

All of the simulations were performed in this study by using quantum-based MD in conjunction with multiscale shock technique (MSST)[34] implemented in the CP2K code. This method is based on the Navier−Stokes equations and combines molecular dynamics and the one dimension (1D) Euler equations to model the propagation of the shock wave for compressible flow. The electronic mechanism of heat conduction is neglected in the high-temperature shock. The Hugoniot relation and Rayleigh line are obtained according to the conservation equations of mass, momentum, and energy across the shock front. Instead of simulating a shock wave within a large computational cell with many atoms, the computational cell of the MSST method follows a Lagrangian

DOI: 10.1021/acs.jpcb.5b05081
J. Phys. Chem. B 2015, 119, 10673−10681

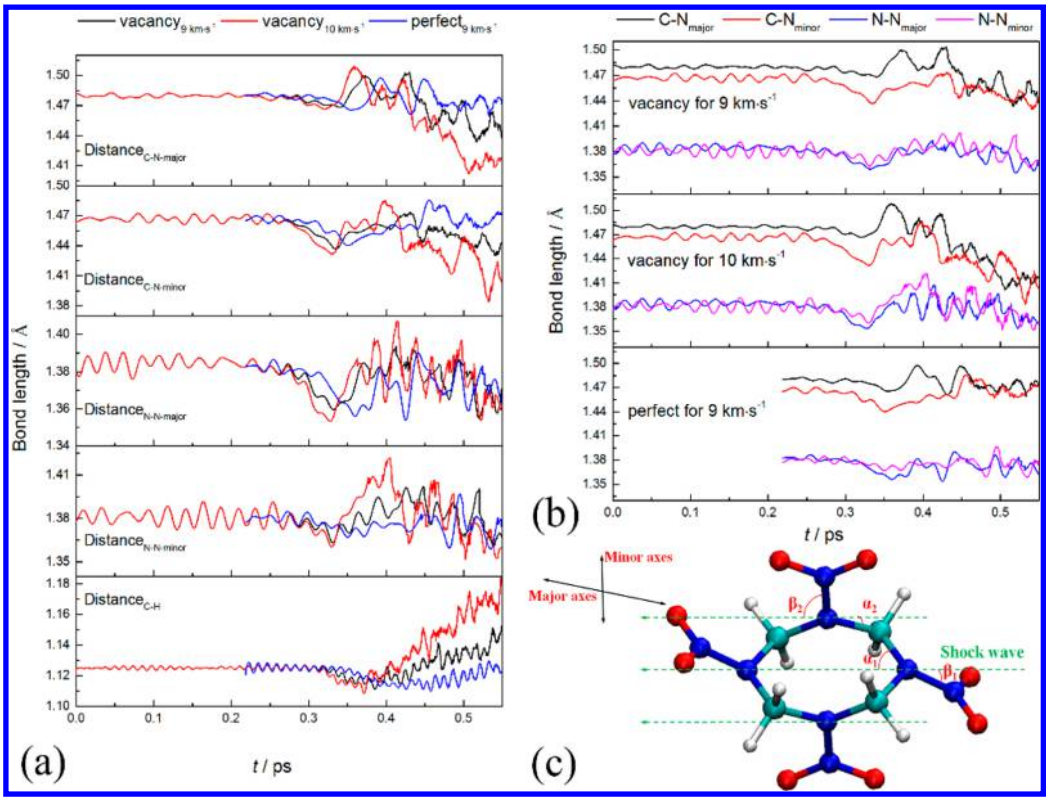

Figure 2. Evolutions of bond length for β-HMX molecule: (a) 9 and 10 km·s^{-1} shocks both in perfect and molecular vacancy models, (b) different changes for the same kind of bond, and (c) angles between bonds and shock direction.

point through the shock wave, enabling the simulation of the shock wave with really fewer atoms and significantly lower computational cost. This technique had been successfully tested on simulating of NM,[35] TATB,[36] and HMX[20,23,29,37] under the shock wave loading and shown to be an accurate prediction of physical and chemical behaviors.

The electronic structure calculations were based on the self-consistent-charge density-functional tight-binding method (SCC-DFTB).[38] This method is based on second-order expansion of the Kohn−Sham total energy in density-functional theory (DFT) with respect to charge density fluctuation, which allows one to describe the total energies, atomic forces, and charge transfer in a self-consistent manner. It was applied to the study of nitromethane and TATB under pressure, which had great consistent results with the other density functional calculations.[36,39]

In this calculation, the crystal structure of the β-HMX original cell was obtained from the experimental data determined by X-ray,[40] which was well-known as a monoclinic molecular crystal structure. The three crystallographic axes constants of the unit cell (a, b, and c) were 6.54, 11.05, and 8.70 Å, respectively. A 5 × 2 × 2 supercell structure was first constructed which contained 40 β-HMX molecules. The cell optimization was carried out, and the lattice parameters were attained as a = 32.379 Å, b = 21.253 Å, c = 17.512 Å, α = 90°, β = 124.02°, and γ = 90°. These calculation results were really in agreement with the experimental data, only with 3.83% difference at the b axis and less than 1.0% difference at a and c axes.

To explore the surface chemistry and more accurately reflect the general reaction condition of HMX, we cut the 5 × 2 × 2 supercell along the (1 0 0) surface to construct a slab model, in which 40 molecules constructed five molecular layers, with 5 Å vacuum along the x-axis (see Figure 1a). The lattice parameters were a = 21.253 Å, b = 17.512 Å, c = 34.143 Å, and α = β = γ = 90°. The (1 0 0) surface was employed along the y−z plane to expose the major N−NO_2 bond[13] to the shock wave, which was considered as the most possible site for the HMX initial decomposition according to previous works.[10,21] For the stress effect of the molecular vacancy, two HMX molecules were taken out of the third layer of the supercell structure (see Figure 1b). Meanwhile, the condition of one-molecule vacancy was also considered for comparison. The N−NO_2 bonds were classified into minor N−NO_2 and major N−NO_2[13] groups for more convenience in comparing the difference dynamic responses later. See Figure 1c; N1−N2 and N5−N6 were the major N−NO_2 groups, while N3−N4 and N7−N8 made up the minor N−NO_2 groups. Also the C−N bonds were distinguished according to the adjacent N atom.

The 5 × 2 × 2 (1 0 0) supercell structure was equilibrated at the temperature of 300 K for 3 ps. And then uniaxial compression of the shock wave was loaded along the x-axis. The fictitious cell mass of 7 × 10^7 au was employed for MSST calculations. The shock speeds of 9 and 10 km·s^{-1} were selected, considering the reasonable and fast shock response condition for the single and pure HMX crystal. The initial temperature and pressure were 300 K and 0 GPa, respectively. The wave function convergence criterion was 10^{-6} au, and the time step of 0.1 fs was selected for all MD calculations. Each MD-MSST calculation was run for 5 ps to completely reveal the dynamic response and initial decomposition process of HMX under shock loading.

In order to check the reliability of our calculations and conclusions, another three MD simulations with different initial configurations were also carried out. The results showed that the dynamic response processes of HMX under shock loading

DOI: 10.1021/acs.jpcb.5b05081
J. Phys. Chem. B 2015, 119, 10673−10681

Table 1. Maximum Compression and Stretch Ratios of the Various Bonds under Shock Loading within 0.4 ps

	compression ratio (%)			stretch ratio (%)		
bonds	vacancy-9	vacancy-10	perfect	vacancy-9	vacancy-10	perfect
$C-N_{major}$	0.79	0.89	1.04	1.37	1.98	1.13
$C-N_{minor}$	2.04	2.38	1.89	0.38	1.30	0.15
$N-N_{major}$	1.80	2.25	1.92	0.43	0.95	0.28
$N-N_{minor}$	1.28	1.50	0.94	0.99	2.80	0.34
C−H	1.22	1.47	1.09	2.44[a]	5.37[a]	0.36[a]

[a]stretch ratio at 0.55 ps of C−H bond (no stretch before 0.4 ps).

were quite consistent with each other. (see Figure S1 in the Supporting Information)

3. RESULTS AND DISCUSSION

When shock loading on the condensed phase β-HMX, the systematic pressure and temperature increased rapidly with the dramatic volume compressing. The shear interaction between two adjacent molecular layers was enhanced. The molecular thermal vibration became stronger as temperature increased. All of the shock responses resulted in the molecular structure deformation, causing nonequilibrium distribution of local charge. The charge transfer and accumulation were extremely crucial for the initial chemical behavior. In this part, the dynamic evolution of bond length was discussed first to predict the primary initial reaction site. The charge transfer behavior was explored to further understand the early decomposition mechanism at the electronic level. After that, the initial decomposition mechanism of β-HMX was summarized to confirm our conclusions and illustrate the significance of the initial reaction to the following intermolecular reaction.

3.1. Evolutions of Bond Length of β-HMX Molecules under Shock Loading. In this part, the evolutions of various bond lengths were analyzed during the early dynamic compression process. The simulation results of different models, perfect crystal with (1 0 0) surface under 9 km·s^{-1} shock and defective crystal with (1 0 0) surface including molecular vacancy at the shock speeds of 9 and 10 km·s^{-1}, were compared. The average lengths of C−N, N−N, and C−H bonds were obtained by calculating the bond lengths of all molecules within the simulation model at the same time. The change of the N−O bond was ignored because of its nonsensitivity for pressure.[16] From the MD trajectories, the first reaction had already started within 0.4 ps for all of the simulations; thus, the following discussion has been primarily focused on the period around 0.4 ps to uncover the physical response process and chemical reaction behavior of HMX at an early compression stage.

Figure 2a shows the changes of bond length for C−N, N−N, and C−H at the shock speeds of 9 and 10 km·s^{-1}, both in the conditions of perfect and defective HMX crystal. All kinds of bond length decreased first during the compression process. The N−N bonds obviously had considerably large compression, especially for the major group, which was consistent with the conclusions drawn in previous studies under the hydrostatic pressure.[13,16] It denoted that the N−N bond was really sensitive to stress. Also, a comparably large compression was observed in the C−N bond close to the minor axis. After that, all of the bond lengths increased dramatically to reach maximum successively. The times of C−N bond close to the major axes reaching their maximum length were obviously earlier than the others in all conditions, which were ∼0.373, 0.359, and 0.392 ps for the condition of the defective crystal under 9 and 10 km·s^{-1} shocks and of the perfect crystal with 9 km·s^{-1} shock, respectively. The followings were the C−N bonds close to the minor axis, the minor $N-NO_2$ bonds, and the major $N-NO_2$ bonds, but no significant differences were observed among these kinds of bond. It represented that the C−N bonds close to the major axis had priority to be activated during the early compression process. The rupture of the molecular ring at that site was the most possible reaction pathway for the initial decomposition of HMX. And that was followed by the homolytic cleavage of $N-NO_2$ bonds. It should be noted that the degree of C−H bond stretch was really considerable after ∼0.4 ps, indicating that C−H bond was activated significantly, and breaking of C−H bond might become the important reaction pathway during the following reaction process.

The diverse dynamic responses of the same kinds of bonds (C−N and $N-NO_2$ groups) were compared according to the major and minor axes groups (see Figure 2b). The C−N bonds close to the major axis had a small compression ratio of 0.79% and considerable stretch ratio of 1.37%. However, the C−N bonds close to the minor axis had obviously a bigger compression ratio of 2.04% and much smaller stretch ratio of 0.38% (see the condition of the defective HMX model with 9 km·s^{-1} shock in Table 1). The same change trends were also observed in other conditions. These phenomena would be explained by the coupling interactions of temperature and pressure. It illustrated that the C−N bonds close to the major axis were nonsensitive to pressure, but beneficial from the temperature increasing with rapid volume compression. When the condensed phase HMX was compressed, raising the stress resulted in a strong shear interaction between molecular layers, causing a local temperature increase (see Figure 3). The high temperature made drastic thermal vibration of the chemical bond, which was beneficial to the initial chemical reaction. When the compressing system obtained the increasing pressure and temperature, the C−N bonds close to the major axis would be stretched and activated more significantly. Then the initial chemical reaction occurred at these sites. After the molecular ring opening, the $N-NO_2$ homolytic cleavage occurred as discussed earlier. The major $N-NO_2$ bonds had a compression ratio of 1.8% and only a 0.43% stretch, while the minor $N-NO_2$ bonds had a smaller compression ratio of 1.28% and a larger stretch ratio of 0.96%. It indicated that the minor $N-NO_2$ bond was possessed of better reaction activity, which would cleave preferentially during the subsequent reaction process.

It should be noted that, with the (1 0 0) surface of β-HMX just faced to the shock direction, the C−N bonds close to the major axes and minor $N-NO_2$ bonds had bigger angles (α_1 and β_2) with the shock direction, which would efficiently avoid the compression of normal stress to the stretching vibration of the

DOI: 10.1021/acs.jpcb.5b05081
J. Phys. Chem. B 2015, 119, 10673−10681

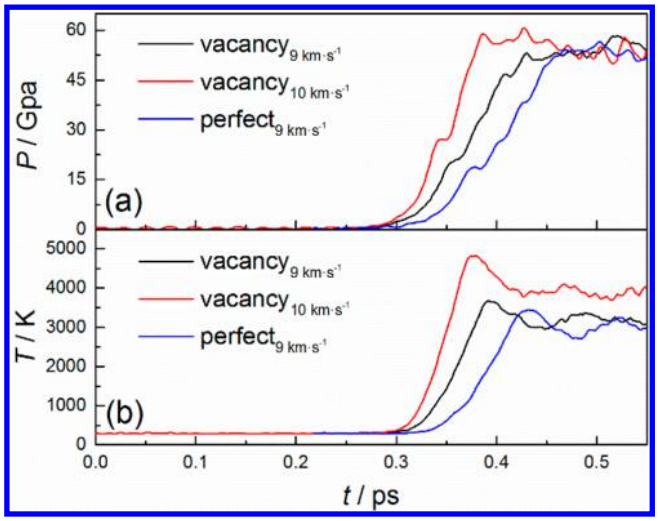

Figure 3. Pressure and temperature evolutions for condensed phase β-HMX.

bonds (see Figure 2c). However, the C−N bonds close to the minor axes and the major N−NO_2 bonds were almost parallel with the shock direction (with smaller angles of α_2 and β_1). The normal stress just suppressed the stretching vibration of these bonds. That was why the diverse response behaviors were observed along the different axes. Namely, the dynamical response behavior clearly depended on the angle between the chemical bond and shock direction. The bonds having a bigger angle (close to 90°) with the shock direction were less sensitive to stress and benefitted more from increasing temperature, which would possess larger stretch performance and better reaction activity during the shock process. Therefore, the initial reaction most likely occurred at the sites, where the chemical bond was nearly vertical to the shock direction.

Also, the effects of shock velocity and defect on the initial response process were compared in detail in Table 1. For the defective HMX models, the condition with shock speed of 10 km·s^{-1} apparently had larger ratios both in the compression and stretch than the condition of 9 km·s^{-1} for all kinds of bond. Apparently, the larger shock speed caused faster compression, resulting in stronger stress on condensed phase HMX (see Figure 3a). Meanwhile, the bigger interaction between molecules caused higher systematic temperature (see Figure 3b), which promoted molecular thermal vibration and chemical bond activation. Thus, the more dramatic stretches of all bonds were observed after compression. Such as the minor axes groups, the N−NO_2 and C−N bonds in the condition of 10 km·s^{-1} almost had three times the stretch ratio as that under the condition of 9 km·s^{-1}. It indicated that, unlike the hydrostatic compression, the higher stress caused by faster shock speed would not result in suppression effect on the C−N and N−NO_2 bond cleavage, because of mechanical and thermodynamic coupling interaction during the compression process. For the conditions of one-molecule vacancy and two-molecule vacancy HMX models, the quite similar evolution processes were obtained. (see Figure S1a,b in the Supporting Information). Compared to the perfect condition with the molecular vacancy HMX condensed phase, despite the clearly smaller pressure loading on the perfect model (see Figure 3a), the slightly bigger compression ratios of 1.04% and 1.92% were obtained for the C−N and N−-NO_2 bonds along the major

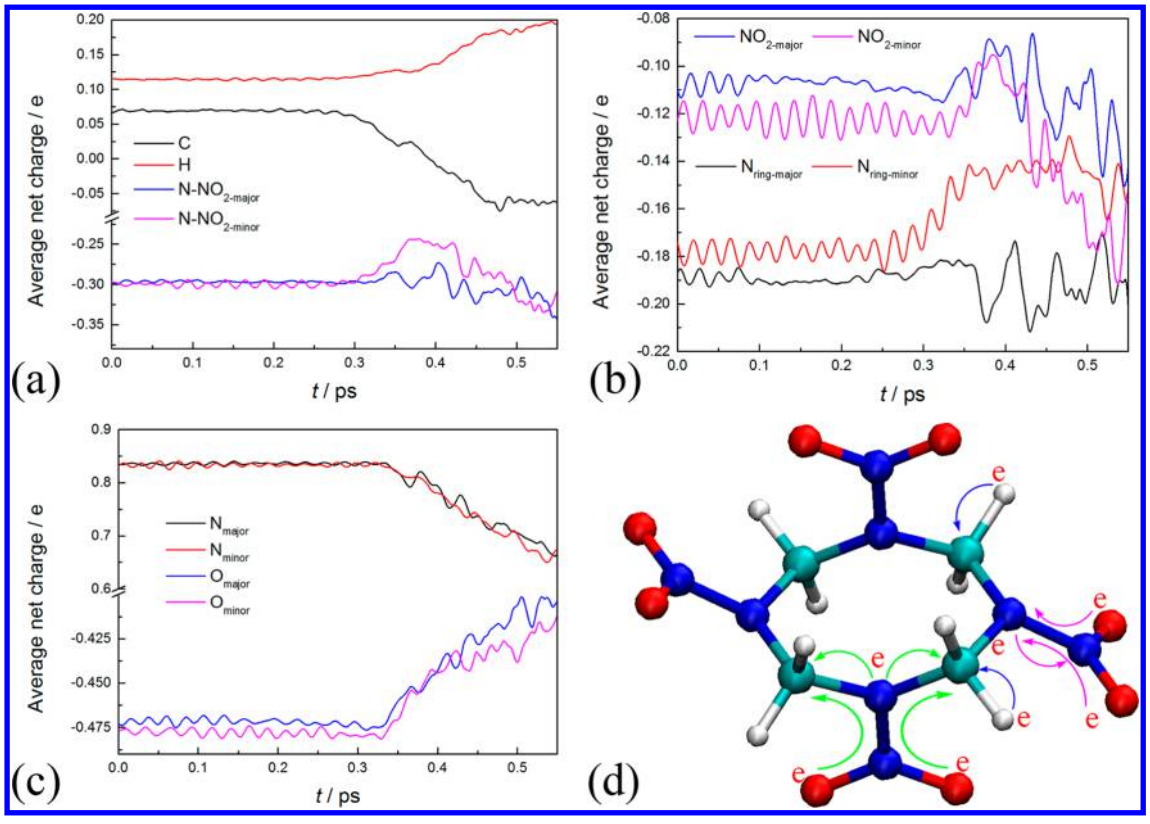

Figure 4. Charge transfer and accumulation for β-HMX with two-molecule vacancy under 9 km·s^{-1} shock loading: (a) charge evolution for whole molecule, (b) charge evolution within N−NO_2 groups, (c) charge evolution within NO_2 groups, and (d) scheme for charge transfer pathway.

DOI: 10.1021/acs.jpcb.5b05081
J. Phys. Chem. B 2015, 119, 10673−10681

axes, respectively. The molecular vacancy obviously reduced the compression effects on the C−N and N−NO_2 bonds. More significantly, the apparently larger stretches for all kinds of bonds were observed in the HMX condensed phase including molecular vacancy. The vacancy also efficiently promoted chemical bond activation and caused initial decomposition occurring around the vacancy more easily.

3.2. Charge Transfer and Accumulation of the β-HMX Molecules under Shock Loading. The molecular structure deformation and chemical bond thermal vibration would cause charge transfer between atoms and instantaneous polarization within bonds and promote the chemical reaction initiation. For more intrinsic understanding of the initial decomposition mechanism proposed earlier, the dynamic charge transfer and accumulation of β-HMX were explored here during the early shock process. The net charge discussed later was average data, coming from all atomic charges within the simulation model at the same time. For simplicity, only the condition of the two-molecule vacancy HMX condensed phase with 9 km·s^{-1} shock was discussed, because of the similar response trends for the different conditions observed in section 3.1.

Figure 4a displayed the main changes of net charge in the different parts of the β-HMX molecule. During the early compression process (before 0.4 ps), the charge was transferred from the group of N−NO_2 and H atom to C atom. This behavior was more apparent between the minor N−NO_2 group and C atom. There was ∼0.058 *e* charge transferred from the minor N−NO_2 group to C atom, while only ∼0.020 and ∼0.022 *e* charge was transferred from the major N−NO_2 group and H atom to C atom, respectively. After ∼0.4 ps, the charge of H atom increased rapidly, while that of N−NO_2 groups decreased correspondingly. A large number of charge was transferred from the H atom to N−NO_2 groups. The interaction between H atom and the N−NO_2 group was enhanced, with the molecular structure further deforming and some initial chemical reactions occurring. This process was more significant for the minor N−NO_2 groups; it was consistent with their larger bond stretch discussed previously.

The diverse charge transfer behaviors were further discussed, within N−NO_2 groups according to different axes. In major N−NO_2 groups, the net charge of NO_2 had a significant increase, while that of N atom in the molecular ring (N_{ring}) decreased correspondingly (see Figure 4b). The charge was first transferred from NO_2 to N_{ring} and then transferred back to the NO_2 group. Only a small portion was transferred to the adjacent C atom through the N_{ring} atom. For the condition of minor N−NO_2 groups, the net charge had an obvious increase both for NO_2 and N atom in the molecular ring. It denoted that the charge was transferred from NO_2 to N_{ring}, and then through the N_{ring} atom to the adjacent C atom. Meanwhile, some charge of N_{ring} atom also was transferred to the adjoining C atom. Figure 4c shows the evolutions of charge within NO_2 groups. The net charge was transferred from the O atom to the nitro N atom, both in the conditions of major and minor NO_2 groups.

From the preceding description, the charge transfer process was summarized as three main pathways during the early compression process. In the major N−NO_2 group, the charge transferred from O atom to the nitro N atom, and then to the connected N atom in the molecular ring. Most of the charge was transferred back to NO_2 group from the N_{ring}; only a little portion was transferred to the adjacent C atom. This process was represented using the pink line in Figure 4d. For the minor N−NO_2 group, the charge was transferred from O atom to nitro N atom, and then all of the charge was transferred to the adjacent C atom through the N_{ring} atom. Some extra charge also was transferred to the C atom from the N_{ring} atom itself (see the green line in Figure 4d). The third pathway was the charge from the H to the C atom. All of the charge transfer processes caused charge accumulating on the C atoms, which was clearly different from that in a previous study[13] on the condition of the hydrostatics. That work proposed that the charge was transferred from H atoms to the N−NO_2 group. However, it was consistent with the following transfer process (after ∼0.4 ps) in our study.

When charge accumulated on the C atom, the electron cloud density increased significantly around the C atom, enhancing the electrostatic shielding to the atomic nucleus. The electronegativity of the C atom was reduced correspondingly. Meanwhile, the charge accumulation was mainly caused by charge transfer from the minor N−NO_2 group, while the major N−NO_2 group had considerable charge density yet. More crucially, the charge transferred from NO_2 to N_{ring} within the major group, as discussed earlier, also resulted in strong electrostatic shielding to the N_{ring} atom. Thus, the electrostatic repulsion between the C atom and the N_{ring} atom in the major N−NO_2 group was really strong, which significantly weakened the C−N interaction. That was why the C−N bond close to the major axes had considerable stretch and activation. Therefore, the HMX decomposition most probably began with the rupture of the C−N bond at that site. For the minor N−NO_2, the total electron cloud density decreased, resulting in weaker interaction between the N−N atoms. More importantly, the electronegativity was enhanced for the NO_2 group, which would promote the electrophilic interaction between the nitro group and the H atom, while, for the major N−NO_2 group, the charge was transferred between the N_{ring} with NO_2 up and down, causing an instantaneous polarization of the N−N bond, which also promoted the chemical bond fission. Thus, both the major and minor N−NO_2 bonds were the potential activation sites. With further compression, the molecular deformation and decomposition enabled H atom and NO_2 to interact with each other, both in intermolecular and intramolecular conditions more readily. The huge charge was transferred from H atom to the nitro O atoms. The fission of the C−H bond would became the important reaction pathway during this period. These conclusions were consistent with the analysis of bond length evolution and gave more intrinsic understanding for the initial decomposition mechanism.

3.3. Initial Reaction Mechanism of β-HMX under Shock Loading. To confirm our analysis methods and conclusions, the initial decomposition mechanism of the two-molecule vacancy condensed phase β-HMX under 9 km·s^{-1} shock loading was analyzed. The first two reaction steps were summarized in Figure 5, and the detailed and main reaction processes were revealed in Figure 6. The first reaction primarily began with the breaking of the C−N bond in the molecular ring. The C−N bonds close to the major axis had obviously an advantage for the initial decomposition (see step 1 in Figure 6). The cleavages of C−H and N−O bond to form the small free radical were observed, which was also reported in previous works.[23,26] But these bonds mostly ruptured by interaction with the other functional groups, such as the interaction between nitro O and H shown in Figure 6, step 2, rather than breaking directly in our work. More interesting, the N−NO_2 bond direct homolytic cleavage occurred near by the molecular vacancy, which further confirmed that the vacancy could supply an

DOI: 10.1021/acs.jpcb.5b05081
J. Phys. Chem. B 2015, 119, 10673−10681

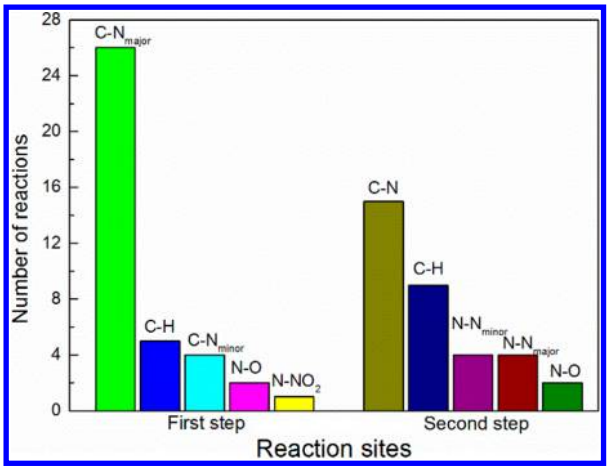

Figure 5. Initial reaction sites for β-HMX with two-molecule vacancy under 9 km·s^{-1} shock loading.

activation space for the bond stretch of the N−NO_2 and promote the reaction that occurred.[22]

The second step reaction was mainly the fission of C−N bond yet causing further cleavage of the molecular ring and generating some small fragments (see step 3 in Figure 6). The homolytic cleavage of the N−NO_2 bonds both in the major and minor axes was another primary reaction pathway, and it was more likely to occur at the adjacent site of the molecular ring gap (see step 4 in Figure 6). After that, the fission of the C−H bond became an important reaction pathway with the interaction of H and NO_2 group being enhanced. This process primarily occurred intermolecularly, and was always induced by electrophilic adsorption of nitro O atom of the small fragment. The reaction process was typically represented using step 5 in Figure 6.

The small fragments discussed earlier were possessed of high reaction activity. Although they might collide and combine to form the longer C−N chain, most of them preferred to interact with each other to generate the main intermediate products through the processes shown in Figure 6, steps 6−8, typically. The terminal nitro would eliminate directly to form NO_2. Also they may interaction with other H-species to produce $^{\bullet}$OH, H_2O, N_2O, and other small C−N fragments. The CO would be generated by the adsorption of terminal C atom and O species. From the preceding analysis, the nitro O atom elimination was an important reaction model for the initial decomposition of HMX, forming some primary free radical, such as $^{\bullet}$OH, which would accelerate the further cleavage of HMX molecule and cause the violent detonation process. More interesting, molecular fragmentation could efficiently enhance the interaction between different molecules and promote this chain reaction occurring.

4. CONCLUSIONS

The microscopic dynamic response and initial decomposition mechanism of β-HMX under shock loading were revealed using quantum-based molecular dynamics (MD) calculation in conjunction with multiscale shock technique (MSST). The evolutions of various chemical bond lengths and charge transfers were analyzed to explore and understand the initial decomposition mechanism of β-HMX. The charge accumulation on C atom, causing stronger electrostatic repulsion interaction between C atom and N−NO_2 close to major axes and enabling the fission of C−N bond to become the most primary model for initial decomposition of HMX. The N−NO_2 bonds stretch and cleavage, caused by the electron density decrease of minor N−NO_2 and charge vibration between N_{ring} and NO_2 of major N−NO_2, were the main reaction pathway after molecular ring breaking. The C−H bond breaking was also an important reaction pathway during the following reaction process, which was mainly induced by electrophilic adsorption of nitro O atom to H atom. This process preferred to occur at intermolecular condition and was clearly promoted by the molecular fragmentation. More importantly, the dynamic response behavior clearly depended on the angle between the

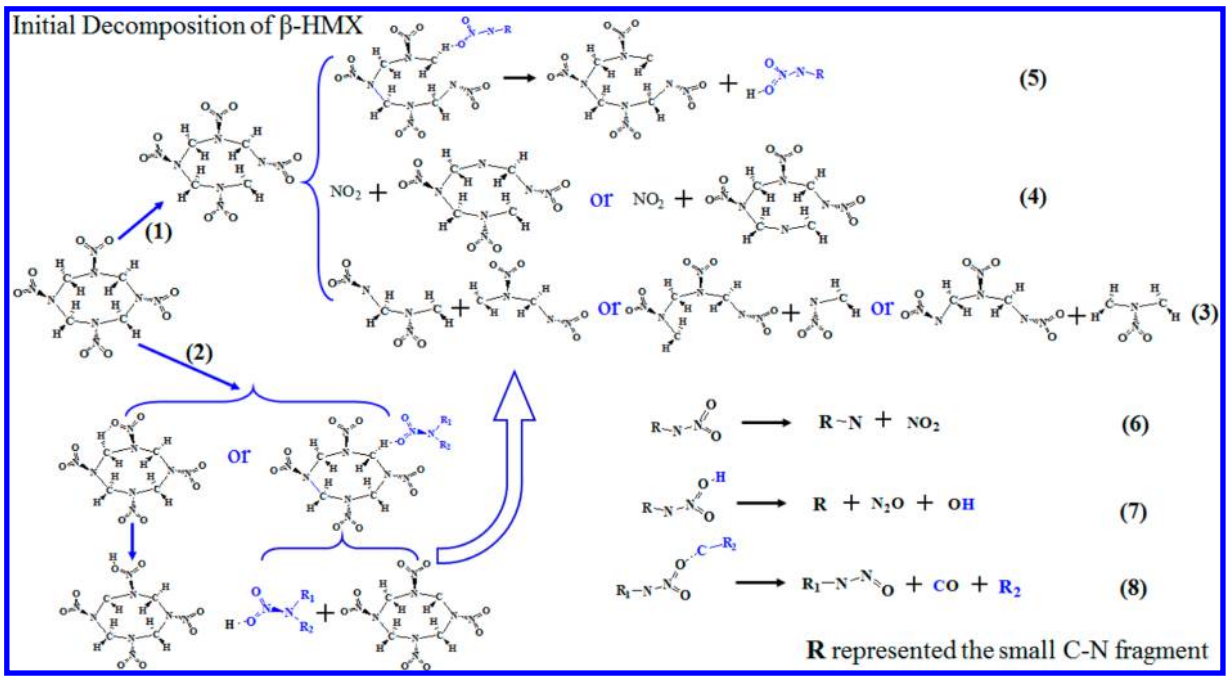

Figure 6. Initial decomposition of β-HMX with two-molecule vacancy under 9 km·s^{-1} shock loading.

DOI: 10.1021/acs.jpcb.5b05081
J. Phys. Chem. B 2015, 119, 10673−10681

chemical bond and shock direction. A bigger angle (close to 90°) enabled the chemical bond to avoid the compression efficiently and get the fast activation with increasing temperature. It was the most potential reaction site for the initial decomposition during the early compression stage.

■ ASSOCIATED CONTENT

Supporting Information

Supplementary figure The Supporting Information is available free of charge on the ACS Publications website at DOI: 10.1021/acs.jpcb.5b05081.

Figure of evolution of bond length for β-HMX (PDF)

■ AUTHOR INFORMATION

Corresponding Authors

*(L.-M.L.) E-mail: limin.liu@csrc.ac.cn. Tel.: 0086-10-82687086.

*(W.-J.Z.) E-mail: wjzhu@caep.cn. Tel.: 0086-0816-2493745.

Notes

The authors declare no competing financial interest.

■ ACKNOWLEDGMENTS

This work was supported by the National Natural Science Foundation of China (Grant No. 51222212), the Basic Research Project of National Defence (Grant No. B1520132013), and the Development Foundation of China Academy of Engineering Physics (Grant Nos. 2014A0101004 and 2013B0101002).

■ REFERENCES

(1) Cooper, P. W.; Kurowski, S. R. *Introduction to the Technology of Explosives*; Wiley: New York, 1996.

(2) Akhaven, J. *The Chemistry of Explosives*; Royal Society of Chemistry: Cambridge, U.K., 1998.

(3) Dlott, D. D. New Developments in the Physical Chemistry of Shock Compression. *Annu. Rev. Phys. Chem.* **2011**, *62*, 575−597.

(4) Yoo, C.-S.; Cynn, H. Equation of State, Phase Transition, Decomposition of β-HMX (Octahydro-1,3,5,7-tetranitro-1,3,5,7-tetrazocine) at High Pressures. *J. Chem. Phys.* **1999**, *111*, 10229−10235.

(5) Main, P.; Cobbledick, R. E.; Small, R. W. H. Structure of the Fourth Form of 1,3,5,7-tetranitro-1,3,5,7-tetraazacyclooctane (γ-HMX), $2C_4H_8N_8O_8.0.5H_2O$. *Acta Crystallogr., Sect. C: Cryst. Struct. Commun.* **1985**, *41*, 1351−1354.

(6) Zhu, W.; Xiao, J.; Ji, G.; Zhao, F.; Xiao, H. First-Principles Study of the Four Polymorphs of Crystalline Octahydro-1,3,5,7-tetranitro-1,3,5,7-tetrazocine. *J. Phys. Chem. B* **2007**, *111*, 12715−12722.

(7) Cooper, P. W. *Explosives Engineering*; Wiley-VCH: New York, 1996.

(8) Sharia, O.; Tsyshevsky, R.; Kuklja, M. M. Surface-Accelerated Decomposition of δ-HMX. *J. Phys. Chem. Lett.* **2013**, *4*, 730−734.

(9) Gump, J. C.; Peiris, S. M. Isothermal Quations of State of Beta octahydro-1,3,5,7-tetranitro-1,3,5,7-tetrazocine at High Temperatures. *J. Appl. Phys.* **2005**, *97*, 053513(1−7).

(10) Sharia, O.; Kuklja, M. M. Modeling Thermal Decomposition Mechanisms in Gaseous and Crystalline Molecular Materials: Application to β-HMX. *J. Phys. Chem. B* **2011**, *115*, 12677−12686.

(11) Zaug, J. M. *Proceedings of the Eleventh International Detonation Symposium*; Office of Naval Research: Arlington, VA, USA, 1998.

(12) Pulham, C. R.; Millar, D. I. A.; Oswald, I. D. H.; Marshall, W. G. *High-Pressure Crystallography: From Fundamental Phenomena to Technological Applications-NATO Science for Peace and Security Series B: Physics and Biophysics*; Springer: New York, 2010.

(13) Peng, Q.; Rahul; Wang, G.; Liu, G.-R.; De, S. Structures, Mechanical Properties, Equations of State, and Electronic Properties of β-HMX under Hydrostatic Pressures: A DFT-D2 study. *Phys. Chem. Chem. Phys.* **2014**, *16*, 19972−19983.

(14) Zhu, W.; Zhang, X.; Wei, T.; Xiao, H. DFT Studies of Pressure Effects on Structural and Vibrational Properties of Crystalline Octahydro-1,3,5,7-tetranitro-1,3,5,7-tetrazocine. *Theor. Chem. Acc.* **2009**, *124*, 179−186.

(15) Wu, Z.; Kalia, R. K.; Nakano, A.; Vashishta, P. Vibrational and Thermodynamic Properties of β-HMX: A First-Principles Investigation. *J. Chem. Phys.* **2011**, *134*, 204509(1−10).

(16) Cui, H.-L.; Ji, G.-F.; Chen, X.-R.; Zhu, W.-H.; Zhao, F.; Wen, Y.; Wei, D.-Q. First-Principles Study of High-Pressure Behavior of Solid β-HMX. *J. Phys. Chem. A* **2010**, *114*, 1082−1092.

(17) Lu, L.-Y.; Wei, D.-Q.; Chen, X.-R.; Lian, D.; Ji, G.-F.; Zhang, Q.-M.; Gong, Z.-Z. The First Principle Studies of the Structural and Vibrational Properties of Solid β-HMX under Compression. *Mol. Phys.* **2008**, *106*, 2569−2580.

(18) Zhou, T.; Song, H.; Liu, Y.; Huang, F. Shock Initiated Thermal and Chemical Responses of HMX Crystal from ReaxFF Molecular Dynamics Simulation. *Phys. Chem. Chem. Phys.* **2014**, *16*, 13914−13931.

(19) Sharia, O.; Kuklja, M. M. Comparative Analysis of Decomposition Reactions in Gaseous and Crystalline β-HMX. *AIP Conf. Proc.* **2012**, *1426*, 1223−1226.

(20) Ge, N.-N.; Wei, Y.-K.; Ji, G.-F.; Chen, X.-R.; Zhao, F.; Wei, D.-Q. Initial Decomposition of the Condensed-Phase β-HMX under Shock Waves: Molecular Dynamics Simulations. *J. Phys. Chem. B* **2012**, *116*, 13696−13704.

(21) Manaa, M. R.; Fried, L. E.; Melius, C. F.; Elstner, M.; Frauenheim, T. Decomposition of HMX at Extreme Conditions: A Molecular Dynamics Simulation. *J. Phys. Chem. A* **2002**, *106*, 9024−9029.

(22) Sharia, O.; Kuklja, M. M. Rapid Materials Degradation Induced by Surfaces and Voids: Ab Initio Modeling of β-Octatetramethylene Tetranitramine. *J. Am. Chem. Soc.* **2012**, *134*, 11815−11820.

(23) Zhu, W.; Huang, H.; Huang, H.; Xiao, H. Initial Chemical Events in Shocked Octahydro-1,3,5,7-tetranitro-1,3,5,7- tetrazocine: A New Initiation Decomposition Mechanism. *J. Chem. Phys.* **2012**, *136*, 044516(1−6).

(24) Chakraborty, D.; Muller, R. P.; Dasgupta, S.; Goddard, W. A. Mechanism for Unimolecular Decomposition of HMX (1,3,5,7-Tetranitro-1,3,5,7-tetrazocine), an Ab Initio Study. *J. Phys. Chem. A* **2001**, *105*, 1302−1314.

(25) Zhou, T.-T.; Huang, F.-L. Effects of Defects on Thermal Decomposition of HMX via ReaxFF Molecular Dynamics Simulations. *J. Phys. Chem. B* **2011**, *115*, 278−287.

(26) Ge, N.-N.; Wei, Y.-K.; Song, Z.-F.; Chen, X.-R.; Ji, G.-F.; Zhao, F.; Wei, D.-Q. Anisotropic Responses and Initial Decomposition of Condensed-Phase β-HMX under Shock Loadings via Molecular Dynamics Simulations in Conjunction with Multiscale Shock Technique. *J. Phys. Chem. B* **2014**, *118*, 8691−8699.

(27) Chaban, V. V.; Fileti, E. E.; Prezhdo, O. V. Buckybomb: Reactive Molecular Dynamics Simulation. *J. Phys. Chem. Lett.* **2015**, *6*, 913−917.

(28) Hua, C.; Zhang, P.-J.; Lu, X.-J.; Huang, M.; Dai, B.; Fu, H. Research on the Size of Defects inside RDX/HMX Crystal and Shock Sensitivity. *Propellants, Explos., Pyrotech.* **2013**, *38*, 775−780.

(29) Wen, Y.; Xue, X.; Zhou, X.; Guo, F.; Long, X.; Zhou, Y.; Li, H.; Zhang, C. Twin Induced Sensitivity Enhancement of HMX versus Shock: A Molecular Reactive Force Field Simulation. *J. Phys. Chem. C* **2013**, *117*, 24368−24374.

(30) Sharia, O.; Kuklja, M. M. Surface-Enhanced Decomposition Kinetics of Molecular Materials Illustrated with Cyclotetramethylene-tetranitramine. *J. Phys. Chem. C* **2012**, *116*, 11077−11081.

(31) Zhang, C.; Li, Y.; Xiong, Y.; Wang, X.; Zhou, M. Acid and Alkali Effects on the Decomposition of HMX Molecule: A Computational Study. *J. Phys. Chem. A* **2011**, *115*, 11971−11978.

(32) Kuklja, M. M.; Tsyshevsky, R. V.; Sharia, O. Effect of Polar Surfaces on Decomposition of Molecular Materials. *J. Am. Chem. Soc.* **2014**, *136*, 13289−13302.

(33) Wang, L.; Tuo, X.; Yi, C.; Wang, X. Ab Initio Calculations of the Effects of H^+ and NH_4^+ on the Initial Decomposition of HMX. *J. Mol. Graphics Modell.* **2008**, *27*, 388−393.
(34) Reed, E. J.; Fried, L. E.; Joannopoulos, J. D. A Method for Tractable Dynamical Studies of Single and Double Shock Compression. *Phys. Rev. Lett.* **2003**, *90*, 235503.
(35) Reed, E. J.; Riad Manaa, M.; Fried, L. E.; Glaesemann, K. R.; Joannopoulos, J. D. A Transient Semimetallic Layer in Detonating Nitromethane. *Nat. Phys.* **2008**, *4*, 72−76.
(36) Manaa, M. R.; Reed, E. J.; Fried, L. E.; Goldman, N. Nitrogen-Rich Heterocycles as Reactivity Retardants in Shocked Insensitive Explosives. *J. Am. Chem. Soc.* **2009**, *131*, 5483−5487.
(37) Ge, N.-N.; Wei, Y.-K.; Zhao, F.; Chen, X.-R.; Ji, G.-F. Pressure-Induced Metallization of Condensed Phase β-HMX under Shock Loadings via Molecular Dynamics Simulations in Conjunction with Multi-scale Shock Technique. *J. Mol. Model.* **2014**, *20*, 2350.
(38) Elstner, M.; Porezag, D.; Jungnickel, G.; Elsner, J.; Haugk, M.; Frauenheim, T.; Suhai, S.; Seifert, G. Self-consistent-charge Density-functional Tight-binding Method for Simulations of Complex Materials Properties. *Phys. Rev. B: Condens. Matter Mater. Phys.* **1998**, *58*, 7260−7268.
(39) Margetis, D.; Kaxiras, E.; Elstner, M.; Frauenheim, T.; Manaa, M. R. Electronic Structure of Solid Nitromethane: Effects of High Pressure and Molecular Vacancies. *J. Chem. Phys.* **2002**, *117*, 788−799.
(40) Cady, H. H.; Larson, A. C.; Cromer, D. T. The Crystal Structure of α-HMX and a Refinement of the Structure of β-HMX. *Acta Crystallogr.* **1963**, *16*, 617−623.

DOI: 10.1021/acs.jpcb.5b05081
J. Phys. Chem. B 2015, 119, 10673−10681